

# bradscholars

## Synthesis of Ce<sup>3+</sup> substituted Ni-Co ferrites for high frequency and memory storage devices by sol-gel route

Item Type	Article
Authors	Sheikh, F.A.;Noor ul Huda Khan Asghar, H.M.;Khalid, M.;Gilani, Z.A.;Ali, S.M.;Khan, N.;Shar, Muhammad A.;Alhazaa, A.
Citation	Sheikh FA, Noor ul Huda Khan Asghar HM, Khalid M et al (2023) Synthesis of Ce <sup>3+</sup> substituted Ni-Co ferrites for high frequency and memory storage devices by sol-gel route. Journal of Alloys and Compounds. 938: 168637.
DOI	<a href="https://doi.org/10.1016/j.jallcom.2022.168637">https://doi.org/10.1016/j.jallcom.2022.168637</a>
Rights	© 2022 Elsevier B.V. All rights reserved. Reproduced in accordance with the publisher's self-archiving policy. This manuscript version is made available under the CC-BY-NC-ND 4.0 license.
Download date	2025-08-27 19:47:46
Link to Item	<a href="http://hdl.handle.net/10454/19309">http://hdl.handle.net/10454/19309</a>

# Synthesis of Ce<sup>3+</sup> substituted Ni-Co ferrites for high frequency and memory storage devices by sol-gel route

Furhaj Ahmed Sheikh<sup>1</sup>, H. M. Noor ul Huda Khan Asghar<sup>1</sup>, Muhammad Khalid<sup>2</sup>, Zaheer Abbas Gilani<sup>1, \*</sup>, Syed Mansoor Ali<sup>3</sup>, Noor-ul-Haq Khan<sup>1</sup>, Muhammad Ali Shar<sup>4</sup>, Abdulaziz Alhazaa<sup>3, \*</sup>

<sup>1</sup>Department of Physics, Balochistan University of Information Technology, Engineering & Management Sciences, Quetta 87300, Pakistan

<sup>2</sup>Department of Physics, University of Karachi, Karachi 75270, Pakistan

<sup>3</sup>Department of Physics and Astronomy, College of Science, P.O. BOX 2455, King Saud University, Riyadh, 11451, Saudi Arabia

<sup>4</sup>Department of Mechanical & Energy Systems Engineering, Faculty of Engineering and Informatics, University of Bradford, Bradford BD7 1DP, United Kingdom

## ABSTRACT

Cerium (Ce<sup>3+</sup>) substituted Ni-Co ferrites with composition Ni<sub>0.3</sub>Co<sub>0.7</sub>Ce<sub>x</sub>Fe<sub>2-x</sub>O<sub>4</sub> (x = 0.0 to 0.20, with step size 0.05) were synthesized by sol-gel method. Face-centered cubic (FCC) spinel structure was revealed by X-ray analysis. The crystalline size was calculated ranging between 17.1-18.8 nm, lattice constant showed a decreasing trend with increase of Ce<sup>3+</sup> contents, furthermore, X-ray density was calculated between 5.30-5.69 g/cm<sup>3</sup>. The two characteristic spinel ferrites absorption bands were seen around 550 (cm<sup>-1</sup>) and 415 (cm<sup>-1</sup>) in Fourier transform infra-red (FTIR) spectroscopy. The microstructural and elemental studies were carried out by field emission transmission electron microscopy (FE-TEM) and energy dispersive X-ray (EDX) respectively, the average particle size was calculated around 21.83 nm. Magnetic studies were performed by vibrating sample magnetometer (VSM), which showed that saturation magnetization M<sub>s</sub> and remanence M<sub>r</sub> decreased with substitution up to x = 0.10 due to small magnetic moment of Ce<sup>3+</sup> than Fe<sup>3+</sup>. The coercivity H<sub>c</sub> increased with substitution up to 908.93 Oe at x = 0.05, then it decreased following the trend of anisotropy constant. The dielectric studies exhibited decrease in dielectric parameters with frequency due to decreasing polarization in material. The dielectric loss was significantly decreased in material at high frequency. The Cole-Cole interpretation exhibited conduction mechanism being caused by grain boundary density. These attributes of Ce<sup>3+</sup> substituted Ni-Co ferrites suggest their possible use in memory storage, switching and high frequency devices like antenna and satellite systems.

**Keywords:** Ni-Co ferrites, Sol-gel method, FE-TEM, Magnetic properties, Dielectric properties, Memory storage devices

1  
2  
3  
4 \*Corresponding author at: Zaheer Abbas Gilani, Department of Physics, Balochistan University of Information  
5 Technology, Engineering & Management Sciences, Quetta 87300, Pakistan,  
6 Email Address: zagiani2002@yahoo.com

7  
8 \*Corresponding author at: Abdulaziz Alhazaa, Department of Physics and Astronomy, College of Science, King  
9 Saud University, Riyadh 11451, Saudi Arabia  
10 Email: aalhazaa@ksu.edu.sa

## 11 **1. Introduction**

12 Among ferrites, spinel ferrites are the class of material having spinel structure i.e.  $[M^{2+}Fe_2^{3+}O_4]$   
13 which are crystallized into FCC structure. These metal cations  $M^{2+}$  (divalent) and  $Fe^{3+}$  (trivalent)  
14 in coordination with oxygen atoms are distributed to tetrahedral (A-site) and octahedral (B-Site)  
15 sites [1]. Spinel ferrites have remarkable structural and electromagnetic properties that leads to  
16 their use in technological devices. In past few decades, the spinel ferrites have gained the attention  
17 of scientists because of their possible use in magnetic sensors, computer components, information  
18 storage and high frequency transformers [2-4].  
19

20  
21  
22  
23  
24  
25  
26  
27  
28  
29  
30  
31  
32  
33  
34  
35  
36  
37  
38  
39  
40  
41  
42  
43  
44  
45  
46  
47  
48  
49  
50  
51  
52  
53  
54  
55  
56  
57  
58  
59  
60  
61  
62  
63  
64  
65  
Some of the ferrites like  $NiFe_2O_4$  and  $CoFe_2O_4$  are most demanding materials owing to their  
exceptional properties like high coercive force, high anisotropy energy, reasonable saturation  
magnetization, high thermal, and mechanical strength [5, 6]. Cobalt ferrite  $CoFe_2O_4$  is an important  
candidate in the family of ferrites that belongs to inverse spinel structure and show high value of  
coercivity [7-9]. Nickel ferrite  $NiFe_2O_4$  belongs to soft ferrites having feeble coercivity and  
saturation magnetization [10]. Both Co and Ni ferrites possess an inverse spinel structural  
formation in bulk, where  $M^{2+}$  occupy B-site and  $Fe^{3+}$  are distributed equally between A and B sites  
[11].

Nickel-Cobalt (Ni-Co) ferrites are significant materials pertaining to their use in electronic  
appliances used in high frequency devices which are mostly utilized in telecommunication [1].  
These Ni-Co ferrites have potential and economical use in circuits involving radio frequencies,  
antenna rods, high quality filters, read-write memory heads and core of transformers [12-15].  
These ferrites can have improved structural, magnetic, and dielectric properties by substituting  
rare-earth ( $RE^{3+}$ ) metals. These ferrites can have improved structural, magnetic and dielectric  
properties by substituting rare-earth ( $RE^{3+}$ ) metals [16]. Spinel ferrites with RE substitution have  
gained interest in the field of material science due to remarkable properties like catalytic,  
magnetic, and infrared [17]. As the magnetic properties of these ferrites strongly rely on Fe-Fe  
interactions  
(3d electrons coupling). By doping  $RE^{3+}$  cations, RE-Fe interactions will lead to the 3d-4f electrons  
coupling, that enhance the magnetic features of ferrites [18]. The appropriate amount of  $RE^{3+}$  ions

1  
2  
3  
4 doping in these ferrites can lead to astonishing variations in structural, electric, magnetic, optical  
5 and dielectric properties [5]. The rare-earth ions substitution produces high resistivity in a material  
6 that can be used as electrical insulator. As rare-earth metal cations possess large ionic radii, they  
7 when substituted with  $\text{Fe}^{3+}$  ions evolve the lattice structure completely and produce distortion and  
8 lattice strain [19]. A few reports have been disclosed in literature that have used rare-earth ( $\text{RE}^{3+}$ )  
10 cations as a substituent to produce nano-crystalline ferrites [7, 18-22]. S.S. Satpute et al. [23]  
11 reported the substitution of  $\text{Y}^{3+}$  cations that strongly influenced the magnetic features of cobalt  
12 ferrites. Addition of  $\text{Y}^{3+}$  led to decrease in magnetic attributes. V. More et al. [24] reported  $\text{Ce}^{3+}$   
13 substituted Ni-Mn-Zn ferrites using auto combustion method. The study revealed strong impact of  
14  $\text{Ce}^{3+}$  on morphological and mechanical characteristics of material.  
15  
16  
17  
18  
19

20  
21  
22 Several techniques are available to prepare nano-ferrites viz. sol-gel [20], co-precipitation [25],  
23 microemulsion [26], and hydrothermal [27], etc. Sol-gel technique is one of the most versatile  
24 approaches that has attracted the attention of researcher recently due to its large scale advantages.  
25 This technique provides simple synthesis of ferrites with great control over stoichiometry, it gives  
26 us homogenous material possessing, chemical stability and small grain size [14, 28, 29]. Sol-gel  
27 process is advantageous over conventional ceramic techniques owing to small energy intake, good  
28 chemically homogenous product, greater reactivity, and low degrees of agglomeration that is liable  
29 to the reduction in losses in a material [14]. Moreover, thermal analysis is not necessarily required  
30 compared to those which need it such as co-precipitation, microemulsion, Pechini method etc.  
31  
32  
33  
34  
35  
36  
37  
38

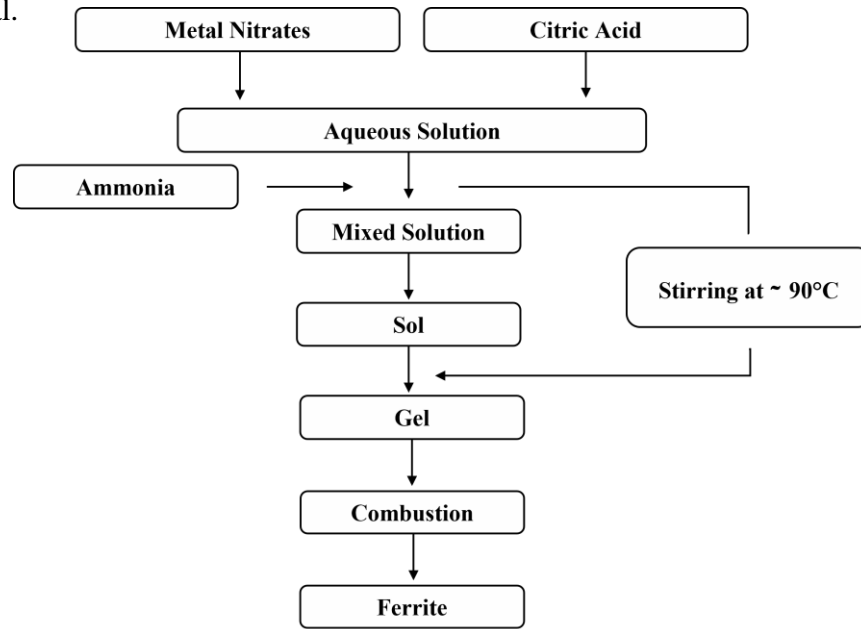
39 In this work, rare-earth metal cerium ( $\text{Ce}^{3+}$ ) substituted Ni-Co ferrite having composition  
40  $\text{Ni}_{0.3}\text{Co}_{0.7}\text{Ce}_x\text{Fe}_{2-x}\text{O}_4$  ( $x = 0.0-0.20$ ) were synthesized by sol-gel technique and the impacts of  $\text{Ce}^{3+}$   
41 substitution on structural, microstructural, magnetic, and dielectric properties were examined.  
42  
43  
44

## 45 2. Experimental

46  $\text{Ce}^{3+}$  substituted Ni-Co ferrites having compositional formula  $\text{Ni}_{0.3}\text{Co}_{0.7}\text{Ce}_x\text{Fe}_{2-x}\text{O}_4$  ( $x = 0.0,$   
47  $0.05, 0.1, 0.15$  and  $0.20$ ) were prepared by sol-gel method. The 99% pure nitrates viz.  
48  $(\text{Ni}(\text{NO}_3)_2 \cdot 6\text{H}_2\text{O})$ ,  $(\text{Co}(\text{NO}_3)_2 \cdot 6\text{H}_2\text{O})$ ,  $(\text{CeN}_3\text{O}_9 \cdot 6\text{H}_2\text{O})$ ,  $(\text{FeN}_3\text{O}_9 \cdot 9\text{H}_2\text{O})$  and citric acid ( $\text{C}_6\text{H}_8\text{O}_7 \cdot$   
49  $\text{H}_2\text{O}$ ) were used to prepare the homogenous solutions. The metal nitrates in addition to citric acid  
50 were used in required proportion with distilled water to prepare sample solutions. Ammonia  
51 solution was added dropwise in these sample solutions to adjust pH to approximately seven. The  
52 solutions were stirred using magnetic stirrer and heated at  $90^\circ\text{C}$  on magnetic hot plates until the  
53 solutions were transformed into a gel. This gel was then heated to  $120^\circ\text{C}$ , and the required product  
54  
55  
56  
57  
58  
59  
60

1  
2  
3  
4 in the form of loose powder was obtained, which was then grinded to get powder samples.  
5 The nano powder was annealed at 600<sup>0</sup>C for 5 hours to get good crystallinity [5, 20]. The  
6 complete  
7

8  
9 synthesis process is presented schematically in Fig. 1. Pallets were prepared with the help of  
10 hydraulic press applying a pressure of 5 tons. Further, the samples were passed through various  
11 characterization techniques. The X-ray diffraction (XRD) patterns of prepared samples were  
12 obtained from PANalytical X'Pert Pro using  $\text{Cu-K}_\alpha$  ( $\lambda = 1.5405 \text{ \AA}$ ) for structural analysis. FTIR  
13 spectroscopy was carried out by NICOLET IS50 to analyze stretching bands of spinel structure.  
14 FE-TEM analysis was performed by JEOL JEM 2100F for detailed study of microstructures. To  
15 study magnetic properties of ferrites, VSM analysis was done by Lakeshore VSM 7400. The  
16 dielectric measurements were performed by LCR meter to study dielectric response of prepared  
17 ferrite material.  
18  
19  
20  
21  
22  
23  
24



25  
26  
27  
28  
29  
30  
31  
32  
33  
34  
35  
36  
37  
38  
39  
40  
41  
42  
43  
44  
45  
46  
47  
48  
49  
50  
51  
52  
53  
54  
55  
56  
57  
58  
59  
60  
61  
62  
63  
64  
65

Fig. 1. Flow chart of sol-gel process

### 3. Results and discussion

#### 3.1. Structural properties

Cerium ( $\text{Ce}^{3+}$ ) substituted  $\text{Ni}_{0.3}\text{Co}_{0.7}\text{Ce}_x\text{Fe}_{2-x}\text{O}_4$  ( $x = 0.0-0.20$ ) were characterized by XRD to study structural properties. The obtained XRD pattern is depicted in Fig. 2, that shows very sharp peaks, the presence of reflection planes (111), (220), (311), (222), (400), (422), (511), (440), (531) and (533) confirmed the formation of FCC spinel structure (space group Fd-3m and space group number 227), the diffraction peaks corresponding to these planes were verified by standard JCPDS

card no. 22-1086 [21, 30]. When  $Ce^{3+}$  substitution was increased the secondary phase appeared in last two samples, that was identified as  $CeO_2$  and matched with standard data card 01-0800. The existence of secondary phase is due to increase in Ce contents. When rare-earth  $Ce^{3+}$  is substituted in Ni-Co ferrites the XRD peaks became less intense and broader. The crystalline grains growth was hindered by  $Ce^{3+}$  ion, which resulted in small grains size. Thus,  $Ce^{3+}$  substituted Ni-Co ferrites have less intense and broader peaks compared to the pure Ni-Co ferrite due to slower growth of crystallites [31].

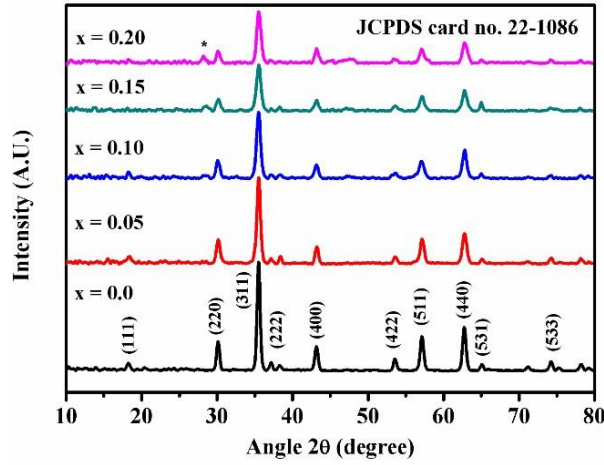


Fig. 2. XRD patterns of  $Ni_{0.3}Co_{0.7}Ce_xFe_{2-x}O_4$  ( $x = 0.0-0.20$ )

The average crystalline size was obtained by following formula [14].

$$D = \frac{k\lambda}{\beta \cos \theta} \quad (1)$$

Where ‘ $k$ ’ is constant, ‘ $\lambda$ ’ is X-ray beam wavelength, ‘ $\beta$ ’ and ‘ $\theta$ ’ denote peak broadening and diffraction angle respectively. The value of crystalline size was lying between 17.1-18.8 nm. The most intense peak was observed nearly at  $2\theta = 35.5^\circ$  having ( $hkl$ ) Miller Indices as (311). The substitution of  $Ce^{3+}$  exhibited broadening of this peak, which eventually points towards the crystals having small particle size. So, the introduction of  $Ce^{3+}$  cations lead towards the decreasing crystalline size up to ( $x \leq 0.15$ ), which happens due to the hindrance in crystalline growth. Similar observation was reported, where substitution of rare-earth metals resulted in decrease of crystalline size [22, 32]. For ( $x = 0.20$ ) the crystalline size increased due to reduction in peak broadening and increase of crystalline growth. Lattice constant was computed by Nelson-Riley function [33].

$$a = d\sqrt{h^2 + k^2 + l^2} \quad (2)$$

Where 'd' represents interplanar spacing and (hkl) are Miller Indices. The lattice constant was determined to be lying between 8.363 to 8.374 Å. It was observed that lattice constant for all the Ce<sup>3+</sup> substituted Ni-Co ferrites was less than the pure one, the highest value of lattice constant was 8.374 Å for (x = 0.0). The lattice constant and cell volume exhibited decreasing trend up to (x = 0.15). As ionic radii of Fe<sup>3+</sup> is 0.67 Å and that of Ce<sup>3+</sup> is 1.14 Å, greater ionic radius of Ce produce lattice distortion and accumulate at grain boundaries, thus restricting the cell parameter growth and decrease the lattice parameter [22, 34]. The smallest value of lattice constant was 8.363 Å reported at (x = 0.15). The cell volume was lying between 585-587 (Å)<sup>3</sup> with smallest value of 585 (Å)<sup>3</sup> for (x = 0.15). For (x = 0.20) lattice parameter increases as a result of increase in concentration of Ce<sup>3+</sup> having larger ionic radius than Fe<sup>3+</sup> following Vegard's law [35]. As Ce<sup>3+</sup> ions possess larger size compared to Ni, Co, and Fe ions, generally accumulate at grain boundaries restricting growth and producing lattice strain in a material thus inducing variations in crystalline size and lattice parameter [35]. At (x = 0.20) lattice parameter enhanced to a value 8.369 Å, this increase is attributed to the Ce<sup>3+</sup> increased contents, as Ce<sup>3+</sup> ions have larger ionic radii than Fe<sup>3+</sup> hence increased lattice parameter for (x = 0.20). Many researchers have reported such kind of variations in crystalline size and lattice parameter [21, 35, 36]. The variations in crystalline size and lattice constant are depicted in Fig. 3.

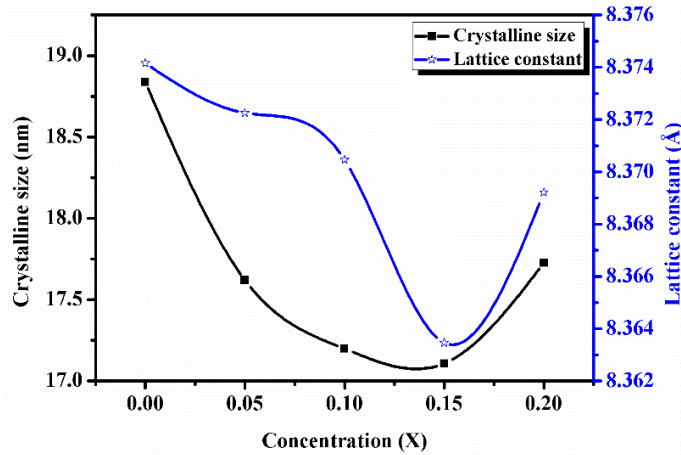


**Fig. 3.** Variations in crystalline size and lattice constant with Ce<sup>3+</sup> concentration

X-ray density was computed to study density of atoms or molecules in a unit cell by using formula [37].

$$\rho_x = \frac{8M}{Na^3} \quad (3)$$

Here ‘ $M$ ’ signifies molecular weight and ‘ $N$ ’ is Avogadro’s number. As atomic weight of  $Ce^{3+}$  (140.116 amu) is greater compared to  $Fe^{3+}$  (55.845 amu), this leads to increase X-ray density in  $Ce^{3+}$  substituted Ni-Co ferrites [7]. Bulk density of prepared ferrites was obtained by using a following relation:

$$\rho_b = \frac{M}{V} \quad (4)$$

Here ‘ $M$ ’ and ‘ $V$ ’ represent mass and volume of prepared sample pallets respectively. The calculation of bulk density showed the dependance on mass of the sample pallet. It was observed that bulk density possessed variations, which was due to the unavoidable pores induced during synthesis and annealing process [37]. The calculated values of X-ray density and bulk density were found to be in the range 5.30-5.69  $g/cm^3$  and 2.58-2.61  $g/cm^3$  respectively. Moreover, other parameters like lattice strain, dislocation density, micro strain, and stacking fault were also calculated to study strains produce and planer defects in a material. All these structural parameters are tabulated in Table 1.

**Table 1.** Structural parameters of  $Ce^{3+}$  substituted Ni-Co ferrites

Parameter	X = 0.00	X = 0.05	X = 0.10	X = 0.15	X = 0.20
Crystalline size D (nm)	18.836	17.620	17.198	17.107	17.725
Lattice constant $a$ (Å)	8.374	8.372	8.370	8.363	8.369
Cell volume (Å) <sup>3</sup>	587.249	586.849	586.473	585.003	586.210
X-ray density $\rho_x$ ( $g/cm^3$ )	5.305	5.404	5.503	5.613	5.697
Bulk density $\rho_b$ ( $g/cm^3$ )	2.5831	2.6145	2.6145	2.5936	2.5936
Lattice strain $\times 10^{-3}$	4.683	6.038	6.686	8.027	8.035
Micro strain $\times 10^{-3}$	1.4293	1.8409	2.0439	2.4513	2.4516
Dislocation density $\times 10^{15}$ (lines/m <sup>2</sup> )	2.818	3.220	3.380	3.416	3.182
Stacking fault	0.789	0.790	0.787	0.788	0.789

These parameters were determined employing the relations [38].

$$Lattice\ strain = \frac{\beta}{4 \tan \theta} \quad (5)$$

$$Microstrain = \frac{\beta \cos \theta}{4} \quad (6)$$

$$\text{Dislocation density} = \frac{1}{D^2} \quad (7)$$

$$\text{Stacking fault} = \frac{2\pi^2}{45\sqrt{3}(\tan \theta)} \quad (8)$$

Analyzing these tabulated values, it is clear that lattice strain and micro strain possess increasing tendency, owing to larger ionic radius of  $\text{Ce}^{3+}$  than  $\text{Fe}^{3+}$ . The increment in strain is because of rise in dislocations, crystal compactness, grain boundaries and micro stresses. In this study dislocation density raised up to ( $x = 0.15$ ), then it decreases with rise in  $\text{Ce}^{3+}$  contents varying inversely as crystalline size [21, 35].

### 3.2. FTIR studies

FTIR spectroscopy is very useful technique to study completion of chemical reaction, formation of spinel structure, deformations due to substitution of ions, and cations distribution. Through this technique the vibrational modes of crystals are studied to interpret the position of ions in lattice [39]. The FTIR spectra of prepared ferrites were taken in span of  $400\text{-}1300\text{ cm}^{-1}$  as depicted in Fig. 4, which confirmed the formation of characteristic spinel ferrite absorption bands ( $\nu_1$ ) and ( $\nu_2$ ) around  $550\text{ (cm}^{-1}\text{)}$  and  $415\text{ (cm}^{-1}\text{)}$  corresponding to tetrahedral and octahedral stretching vibrations respectively, presence of these bands designates the successful development of FCC spinel structure [40, 41].

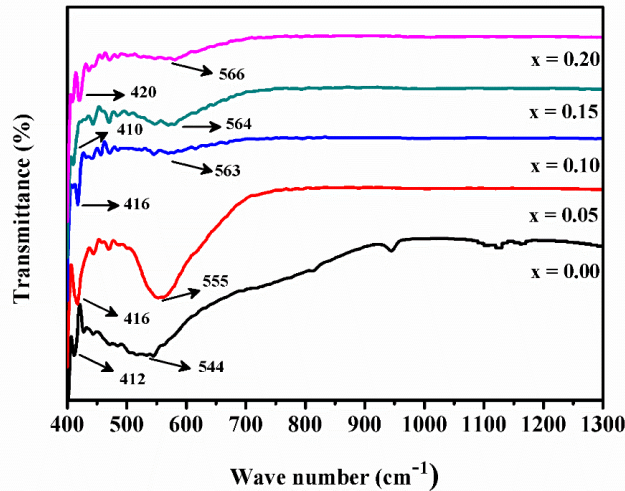


Fig. 4. FTIR spectra of  $\text{Ni}_{0.3}\text{Co}_{0.7}\text{Ce}_x\text{Fe}_{2-x}\text{O}_4$  ( $x = 0.0\text{-}0.20$ )

The frequency band around  $550\text{ (cm}^{-1}\text{)}$  correspond to tetrahedral complexes called high frequency band, while that of around  $415\text{ (cm}^{-1}\text{)}$  correspond to octahedral complexes called low

frequency band, which are summarized in Table 2 [42]. It was observed that these bands were shifted to higher values up on increase of substituent. This shift points towards increase in bond length and eventually confirms the presence of  $Ce^{3+}$  substituted ions [5, 40, 43]. For ( $x \geq 0.10$ ) decrease in intensity of absorption bands was observed, which was due to distortion induced by rearrangement of cations in A and B-sites [44]. Further, the force constants  $K_t$  and  $K_o$  along with tetrahedral and octahedral radii  $R_{tetra}$  and  $R_{octa}$  were calculated and summarized in Table 2. The following relations were used to find these parameters [40].

$$K_o = \frac{0.942128 (M v_2^2)}{M + 32} \quad (9)$$

$$K_t = \sqrt{2} K_o \frac{v_1}{v_2} \quad (10)$$

$$R_{tetra} = a \sqrt{3} (u - 0.25) - R_o \quad (11)$$

$$R_{octa} = a \left( \frac{5}{8} - u \right) - R_o \quad (12)$$

In equation (9) and (10) ' $K_o$ ' is octahedral, and ' $K_t$ ' is tetrahedral force constant, ' $v_1$ ' and ' $v_2$ ' are frequency bands and ' $M$ ' is samples molecular weight. The force constants enhance with the concentration of  $Ce^{3+}$  due to strengthening of inter-ionic bonding. Equation (7) and (8) were employed to calculate tetrahedral and octahedral radii, where ' $u$ ' is oxygen position parameter  $u = 0.375$  and ' $R_o$ ' is oxygen atoms radius  $R_o = 1.32 \text{ \AA}$  [40, 45, 46].

**Table 2.** FTIR parameters of  $Ce^{3+}$  substituted Ni-Co ferrites

Concentration (X)	$v_1$ (cm <sup>-1</sup> )	$v_2$ (cm <sup>-1</sup> )	$K_o$ (dyne/cm) $\times 10^5$	$K_t$ (dyne/cm) $\times 10^5$	$R_o$ (Å)	$R_t$ (Å)
0.00	544	412	1.407218	2.627714	0.773538	0.493057
0.05	555	416	1.437721	2.712622	0.773063	0.492645
0.10	563	416	1.440674	2.757374	0.772616	0.492258
0.15	564	410	1.402197	2.727842	0.770866	0.490743
0.20	566	420	1.474263	2.809682	0.772302	0.491987

### 3.3. FE-TEM and EDX analysis

The microstructural and elemental examination of prepared ferrite nanoparticles were carried out by FE-TEM and EDX studies. FE-TEM micrographs of  $Ni_{0.3}Co_{0.7}Ce_xFe_{2-x}O_4$  for ( $x = 0.15$ ) are depicted in Fig. 5.

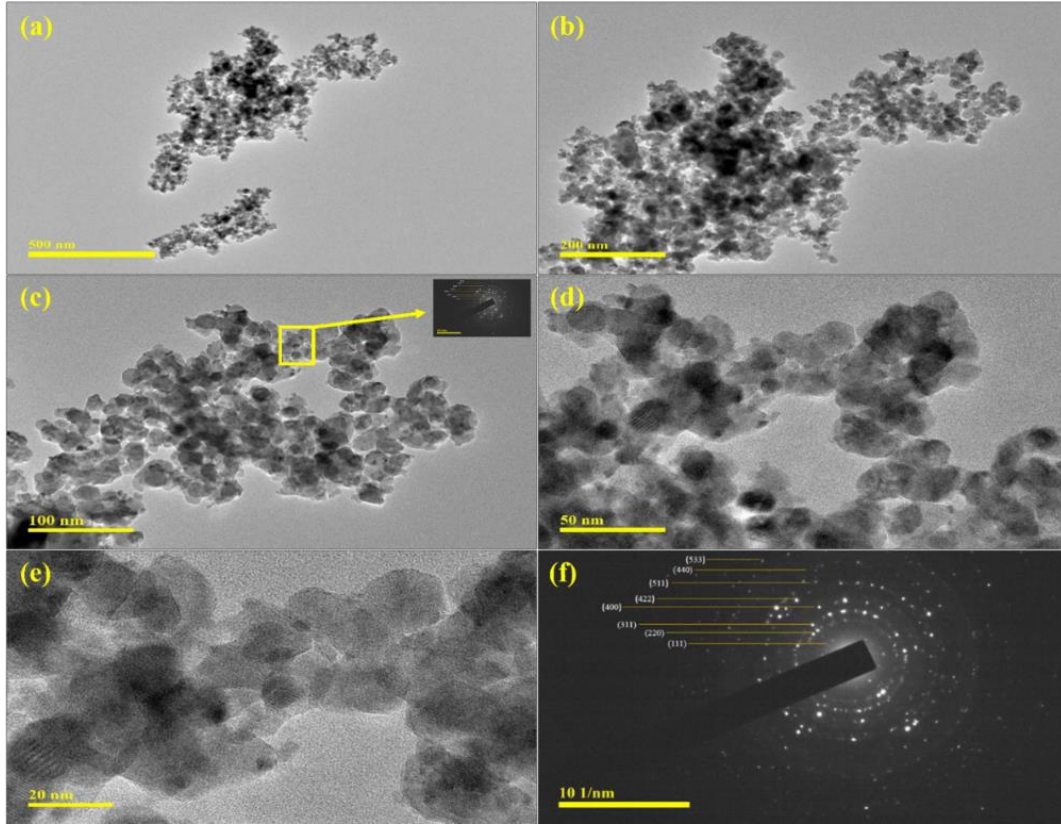


**Fig. 5.** FE-TEM micrographs of  $\text{Ni}_{0.3}\text{Co}_{0.7}\text{Ce}_x\text{Fe}_{2-x}\text{O}_4$  for ( $x = 0.15$ ) with SAED pattern

As there exist strong magnetic interaction between particles, so they appeared to be agglomerated at low magnification [21]. The Fig. 5 (a) and (b) shows clear image of agglomerated particles. The highly magnified micrographs showed that grains possess spherical and cubic symmetry in synthesized samples which can be observed in Fig. 5 (c), (d), and (e). The average particle size estimated was nearly equal to 21.83 nm. The SAED pattern depicted the intense bright ring of (311) plane attributable to development of spinel ferrite. Moreover, the appearance of diffraction rings corresponding to planes (111), (220), (311), (400), (422), (511), (440) and (533) exhibited the development of cubic structure illustrated in Fig. 5 (f). The formation of distinctive rings exhibited the polycrystalline nature of ferrite samples [1, 5]. These rings were indexed using (JCPDS card no. 22-1086) same as used in XRD. The EDX spectra presented in Fig. 6 (a)-(e) confirmed Ni, Co, Ce, Fe and O presence without impurity. The extra Au peaks can be seen in EDX spectra, that is owing to thin gold coating on samples surface to make them conducting, no evidence of any other peak was found [47]. It reveals that the samples are free of contamination.

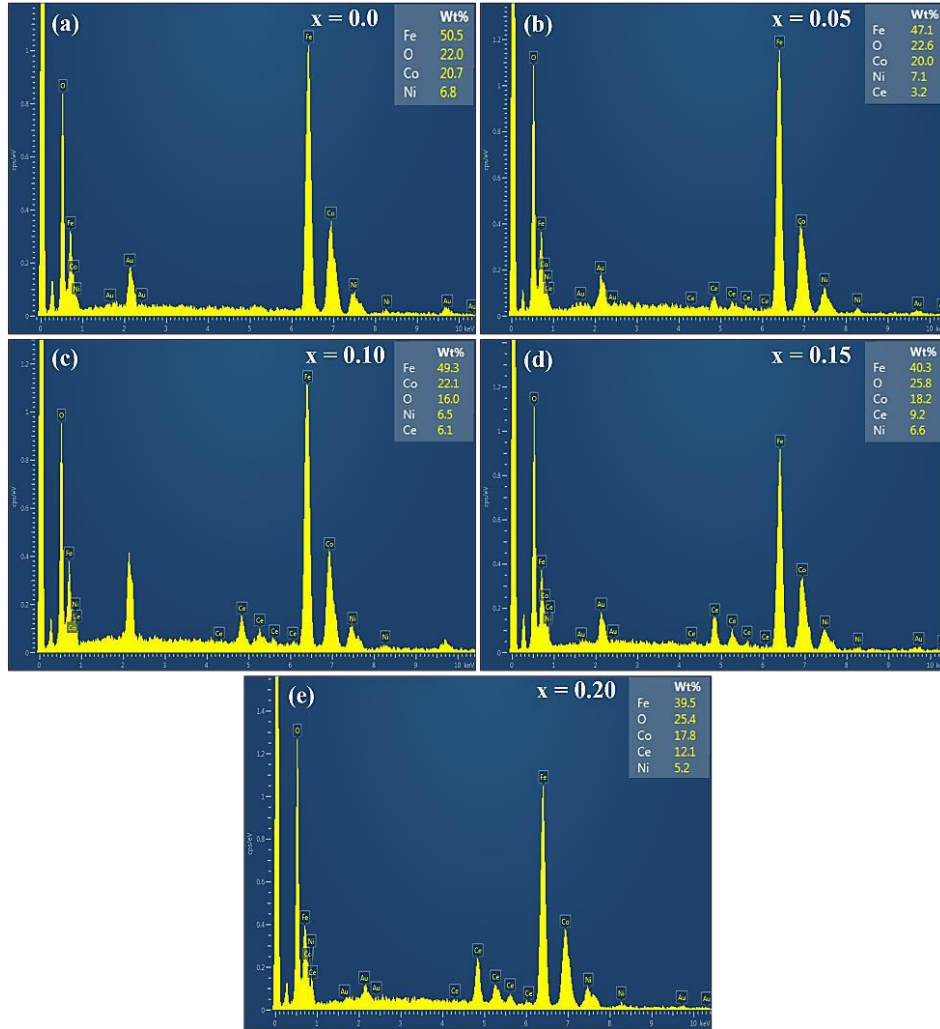


**Fig. 6 (a)-(e).** EDX spectra of  $\text{Ce}^{3+}$  substituted Ni-Co ferrites with weight percentage of elements

The elemental analysis of prepared samples gives the weight percentage of each of these elements as depicted in EDX spectra. With the help of these spectra, it is proved that  $\text{Ce}^{3+}$  contents were enhanced with amount of substitution from  $x = 0.00$  to  $0.20$ , given by weight percentage of cerium that is in continuous increasing trend thus verified its successful substitution.

### 3.4. Magnetic properties analysis

Magnetic properties of  $\text{Ni}_{0.3}\text{Co}_{0.7}\text{Ce}_x\text{Fe}_{2-x}\text{O}_4$  nano-crystalline ferrites were studied at room temperature. The hysteresis curve of these ferrites is illustrated in Fig. 7. The values of  $M_s$ ,  $M_r$ , and  $H_c$  were determined from hysteresis curve. The room temperature magnetization study revealed ferrimagnetic nature of  $\text{Ce}^{3+}$  substituted Ni-Co ferrites.

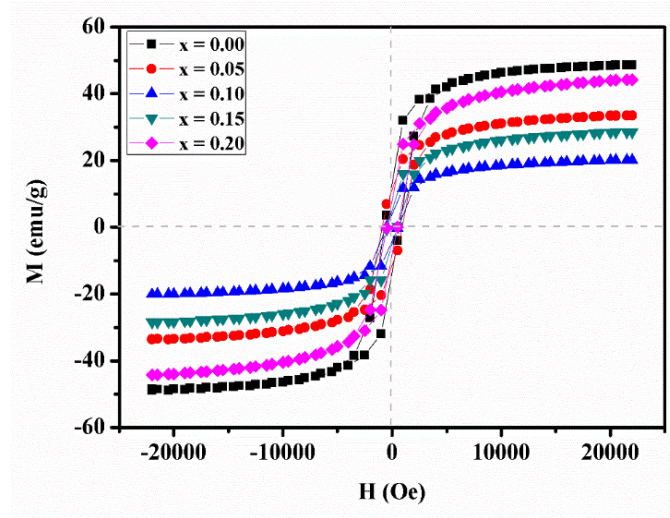


**Fig. 7.** M-H curve of  $\text{Ni}_{0.3}\text{Co}_{0.7}\text{Ce}_x\text{Fe}_{2-x}\text{O}_4$  ( $x = 0.0-0.20$ )

The Fig. 8 (a) shows the variations in  $M_s$  and  $M_r$  values as function of  $\text{Ce}^{3+}$  concentration. It can be observed that  $M_s$  followed decreasing trend up to ( $x = 0.10$ ), then it enhances for further addition of substituent. Similar trend has been observed in  $M_r$  values. Normally,  $\text{Fe}^{3+}$  ions have greater magnetic moment than  $\text{RE}^{3+}$  ions, thus their substitution results decrease in magnetization. This situation can be reversed when magnetic moment of  $\text{RE}^{3+}$  ions become greater than  $\text{Fe}^{3+}$  ions, but this behavior is not seen in all  $\text{RE}^{3+}$  substituted ferrites. It is noted that  $\text{RE}^{3+}$  ions preferably occupy octahedral B-site when substituted in ferrites [31, 48]. In this study, the  $M_s$  and  $M_r$  show decreasing trend from ( $x = 0.0$ ) to ( $x = 0.10$ ), which is due to the replacement of  $\text{Fe}^{3+}$  ions possessing enormous magnetic moment ( $5 \mu_B$ ) by  $\text{Ce}^{3+}$  ions having magnetic moment ( $2.2 \mu_B$ ) [49, 50]. In spinel ferrite nanoparticles the A-A and B-B sublattices have parallel arrangements but the A-B sublattices possess antiparallel arrangement that produce ferrimagnetic order. The residence of  $\text{Fe}^{3+}$  ions at octahedral B-site has significant contribution to magnetic properties of material. As  $\text{Ce}^{3+}$  ions have less magnetic moment than  $\text{Fe}^{3+}$  ions, this results in lessening of super exchange interactions. As far as  $\text{Ce}^{3+}$  concentration is increased from ( $x = 0.10$  to  $0.20$ ), the  $M_s$  value enhanced because of migrating  $\text{Ni}^{2+}$  ions from B to A-site. The  $\text{Ni}^{2+}$  ions tend to occupy tetrahedral site due to partially inverse spinel structure of nickel ferrites compared to perfect inverse spinel cobalt ferrites. So,  $\text{Ni}^{2+}$  ions can be compelled to migrate from B to A-site, as a consequence saturation magnetization increases, same pattern is also reported in literature [21].

The variation in coercivity  $H_c$  and squareness ratio  $M_r/M_s$  is portrayed in Fig. 8 (b). It is noticed that variation in  $H_c$  depend on several parameters such as magnetic anisotropy, grain/particle size,

magnetic domains, micro-strain etc [44, 51, 52]. The substitution of  $Ce^{3+}$  ions in Ni-Co ferrite produce lattice distortion thereby producing anisotropy in a material which leads to greater  $H_c$  values compared to pure Ni-Co ferrites. It is observed that  $H_c$  initially increases for ( $x = 0.05$ ) attaining maximum value of 908.93 Oe, then it decreases for further  $Ce^{3+}$  substitution. This behavior can be related to the anisotropy of the prepared ferrite material [1]. The values of  $H_c$  are calculated to be varying between 461-909 Oe. The  $M_r/M_s$  values were calculated to be in the range 0.17-0.34 and were noted to be less than '1' denoting single domain structure and these low values show decreased exchange interactions in these ferrites [19].

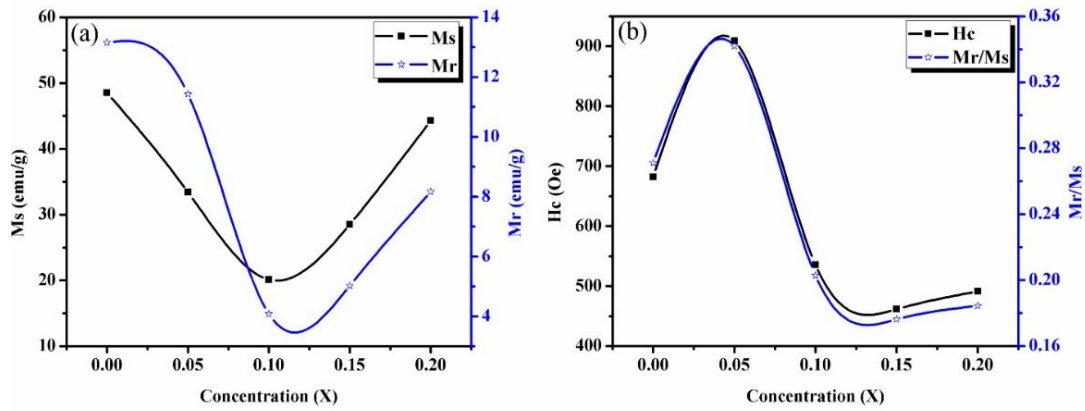


**Fig. 8.** Variations in (a)  $M_s$  and  $M_r$ , (b)  $H_c$  and  $M_r/M_s$  with  $Ce^{3+}$  concentration

The anisotropy constant of prepared ferrite was calculated by using formula [5, 53].

$$H_c = \frac{0.96K}{M_s} \quad (13)$$

Where  $H_c$  represents coercivity and  $M_s$  represents saturation magnetization. Fig. 9 portrays variations in magneto-crystalline anisotropy constant ( $K$ ) with concentration of  $Ce^{3+}$ . The anisotropy constant of material was found to be in the range of 11,220.15-34,471.80 erg/cm<sup>3</sup>. It is observed that ' $K$ ' followed decreasing trend up to ( $x = 0.10$ ) then it rises for further increment in substitution. This decrease in value of ' $K$ ' is due to the distortion induced in ferrites because of  $Ce^{3+}$  substitution. As we are aware about the fact that in Ni-Co ferrites the presence of  $Ni^{2+}$  and  $Co^{2+}$  cations at octahedral B-site are accountable for anisotropy. As the concentration of substituent increases,  $Ni^{2+}$  ions may be drifted from B to A-site. Thus, reduction in  $Ni^{2+}$ - $Co^{2+}$  ions at octahedral site resulted in diminution of anisotropy constant [5].

The Neel's model of A and B sublattices explains magnetic characteristics of material. According to it, super-exchange interactions are present between A-A, A-B and B-B sublattices, the A-B interaction is stronger than the others [54]. The magnetic moment, that is magneton number ( $n_B$ ) of these ferrites was calculated using following relation [21].

$$n_B = \frac{M \times M_s}{5585} \quad (14)$$

In above equation ' $M$ ' represents molecular weights of prepared samples and ' $M_s$ ' shows saturation magnetization. Just like saturation magnetization, the magneton number also followed the same trend, it initially decreased up to ( $x = 0.10$ ), for further increase in substitution its values are also increased, as depicted in Fig. 9. [5, 21].

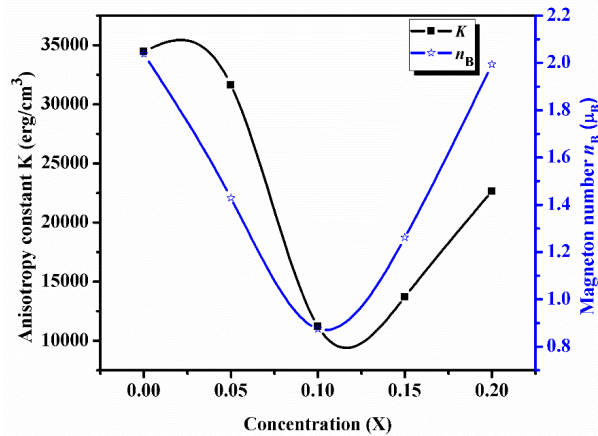


Fig. 9. Variations in  $K$  and  $n_B$  with  $Ce^{3+}$  concentration

### 3.5. Dielectric properties analysis

Several dielectric parameters of prepared nanocrystalline ferrites were computed in applied field frequency (1 MHz-3 GHz) range. Ferrites possess dielectric features due to their preparatory method, crystalline size, and cationic distribution. The dielectric characteristics of ferrites are essential for their applicability in many electronic devices such as filters, antenna rods and high frequency appliances [19].

#### 3.5.1. Variations in dielectric constant, loss, and tangent loss

The dielectric parameters such as dielectric constant, dielectric loss and tangent loss were calculated with respect to applied field frequency. The behavior of dielectric constant seemed to be abruptly decreasing at low frequency and at high frequency slow reduction was observed. Rapid reduction in dielectric constant at small frequency led towards dielectric dispersion. Which is

owing to space charge polarization that is the result of existing highly conducting grains and poorly conducting grain boundaries that cause localized aggregation of charge carriers. The Maxwell-Wagner model of interfacial polarization with Koop's theory explain dispersion of dielectric constant [40, 55, 56]. In ferrites the process of polarization is like a conduction process. Ferrites are known to be dipolar in nature because of  $\text{Fe}^{2+}$  and  $\text{Fe}^{3+}$  ions. The orientational polarization produces because of the rotational motion in dipoles  $\text{Fe}^{2+} \leftrightarrow \text{Fe}^{3+}$  that can be called as electronic exchange. Thus, dipoles align in reaction to applied alternating field and resulting maximum polarization in a material. As the frequency increases polarization decreases in strength because of the fact that electronic exchange cannot obey the applied alternating field above certain frequency [57]. In these  $\text{Ce}^{3+}$  substituted Ni-Co ferrites the  $\text{Ce}^{3+}$  occupy octahedral B-site as having large ionic radius, thus reducing  $\text{Fe}^{3+}$  ions at B-site, that bear significant role in process of polarization. As  $\text{Fe}^{3+}$  ions are reduced at B-site, the polarization decreases due to the hindrance in  $\text{Fe}^{2+}$  and  $\text{Fe}^{3+}$  electronic exchange. Therefore, the dielectric constant reduced with  $\text{Ce}^{3+}$  substitution [58]. With the increase in frequency small resonance peak appeared at 1.8 GHz owing to intrinsic feature of spinel ferrite. When applied frequency and electron's rotational frequency became identical then resonance occurred, which indicated space charge polarization effect. With further increase of frequency to higher values because of electronic and atomic polarizations high resonance occurred at 2.5 GHz. The appearance of these resonance peaks is because of  $\text{Fe}^{2+}$  and  $\text{Fe}^{3+}$  ions residing at B-site creating oxygen vacancies. The pure  $\text{Ni}_{0.3}\text{Co}_{0.7}\text{Fe}_2\text{O}_4$  possessed dielectric constant value of 3.85 at 1 GHz, whereas its value was reduced to 3.02 at the same frequency for  $\text{Ni}_{0.3}\text{Co}_{0.7}\text{Ce}_{0.20}\text{Fe}_{1.8}\text{O}_4$ , this reduction suggests potential use of prepared material in high frequency devices [59].

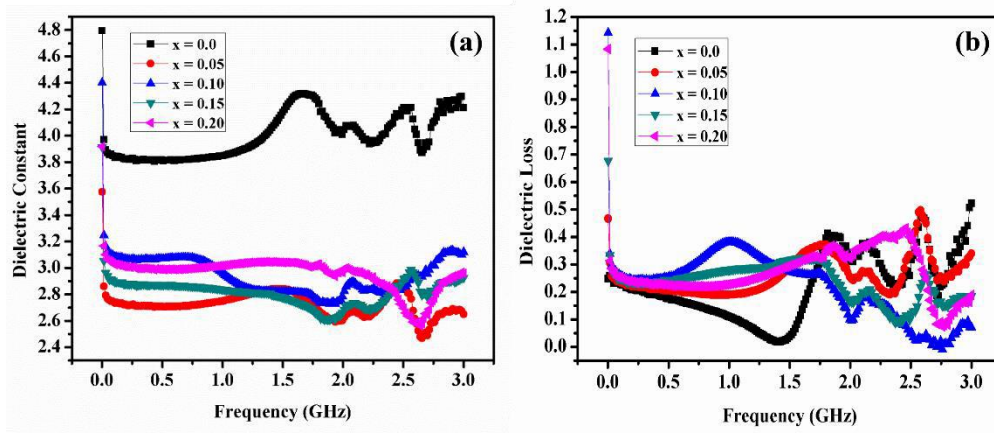


**Fig. 10.** Variations in (a) Dielectric constant and (b) Dielectric loss *versus* frequency

The dielectric loss in material occurs because of electron hopping and defects in dipole. At low frequency the electron hopping is successful, so the dielectric loss is high, as the frequency increases electron hopping is decreased, so is the dielectric loss [40]. The Figs. 10 (a) and (b) portray the variations in these parameters with frequency. The Fig. 11 illustrates the variations in tangent loss. The tangent loss in material appears to be decreasing with increasing frequency because of the strong relation between conduction mechanism and dielectric behaviors. When the hopping frequency and applied field frequency become identical then maximum loss was observed [40].

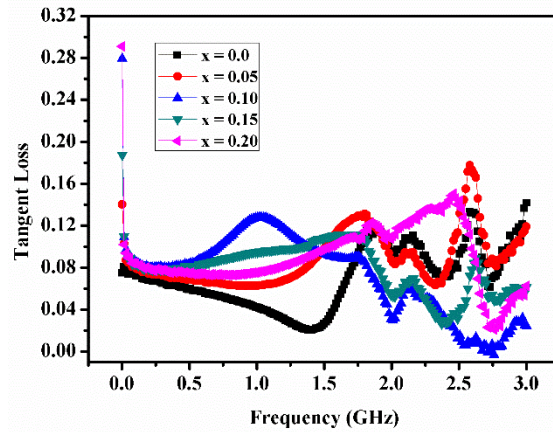


Fig. 11. Tangent loss versus frequency

### 3.5.2. Variations in AC conductivity

The variations in AC conductivity of ferrites with applied frequency is depicted in Fig. 12. AC conductivity was computed using the relation [60].

$$\sigma_a = \frac{t}{A} \frac{Z'}{Z'^2 + Z''^2} \quad (15)$$

Where 't' and 'A' represent thickness and area of pallet, Z' and Z'' represent impedance parts. With increasing applied field frequency, the conductivity also has an increasing trend, which is attributed to the enhancement in electron hopping frequency. With further increase of frequency to a higher range, a dispersive behavior is observed. At 3 GHz the value of conductivity for (x = 0.0) was  $3.39 \times 10^{-2} \Omega^{-1}m^{-1}$  compared to  $3.30 \times 10^{-5} \Omega^{-1}m^{-1}$  at 1 MHz frequency. This increasing trend in AC conductivity is due to small polaron hopping class of conduction phenomenon [40]. The Maxwell-Wagner model with Koop's theory describe that ferrite consists of highly conductive grains divided by resistive grain boundaries. That is why at low frequency region almost all the samples possessed plane behavior owing to grain boundaries high resistance

in this region. At high frequency hopping of charges and the grain effect led to increased values of conductivity. At extremely high frequency due to conducting grains dispersion behavior was observed [61].

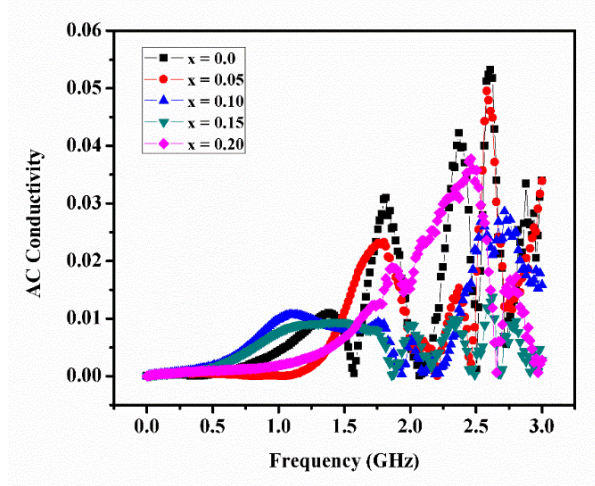


Fig. 12. AC conductivity *versus* frequency

### 3.5.3. Impedance analysis

The Figs. 13 (a) and (b) demonstrate the variations in real ( $Z'$ ) and imaginary ( $Z''$ ) impedance parts with applied frequency respectively. As the frequency rise, their values decrease rapidly and all the impedance curves merge together so that their values nearly remain constant at higher values of frequency, this is because of liberation of space charges. Which are produced due to the inhomogeneity in applied field and variations in concentration. This reduction in  $Z'$  and  $Z''$  with frequency evident an increase in conductivity of material [60].

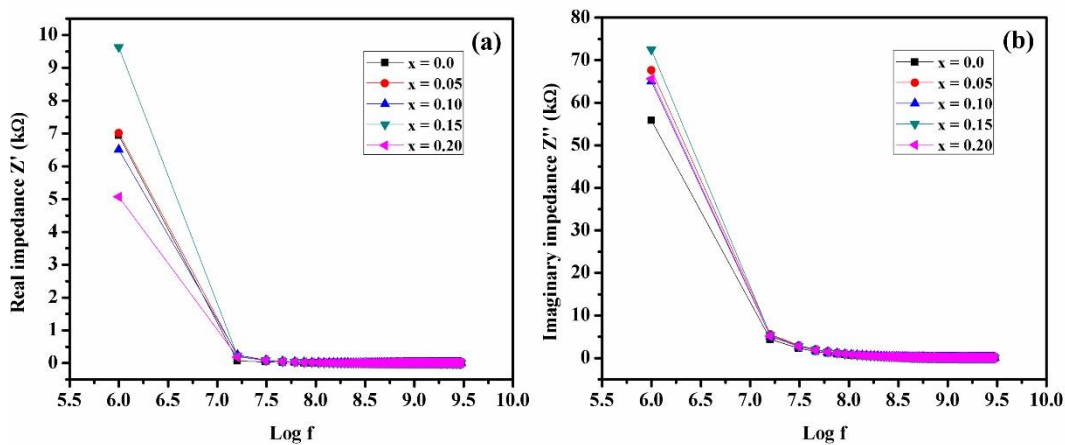


Fig. 13. Variations of (a)  $Z'$  and (b)  $Z''$  *versus* Log f

### 3.5.4. Real and imaginary electric modulus with Cole-Cole study

The real ( $M'$ ) and imaginary ( $M''$ ) electric modulus of ferrite nanoparticles were computed using the relations given below [60].

$$M' = \frac{\varepsilon'}{\varepsilon'^2 + \varepsilon''^2} \quad (16)$$

$$M'' = \frac{\varepsilon''}{\varepsilon'^2 + \varepsilon''^2} \quad (17)$$

Figs. 14 (a) and (b) demonstrate the fluctuations in  $M'$  and  $M''$  respectively within 1 MHz-3 GHz frequency range. We can see that real electric modulus exhibited an increasing behavior with applied frequency. When  $\text{Ce}^{3+}$  concentration is increased,  $M'$  tends to increase with frequency, which is attributed to the space charge polarization in a synthesized material. At certain value of frequency,  $M'$  decrease and then finally increase with frequency. To study space charge effect in a material depending on the applied frequency, the imaginary electric modulus study was done. We can see that  $M''$  decreases with rise in frequency. As  $\text{Ce}^{3+}$  concentration increases in Ni-Co ferrites, the value of  $M''$  enhanced up to a certain value of applied frequency then it followed a decreasing trend [40].

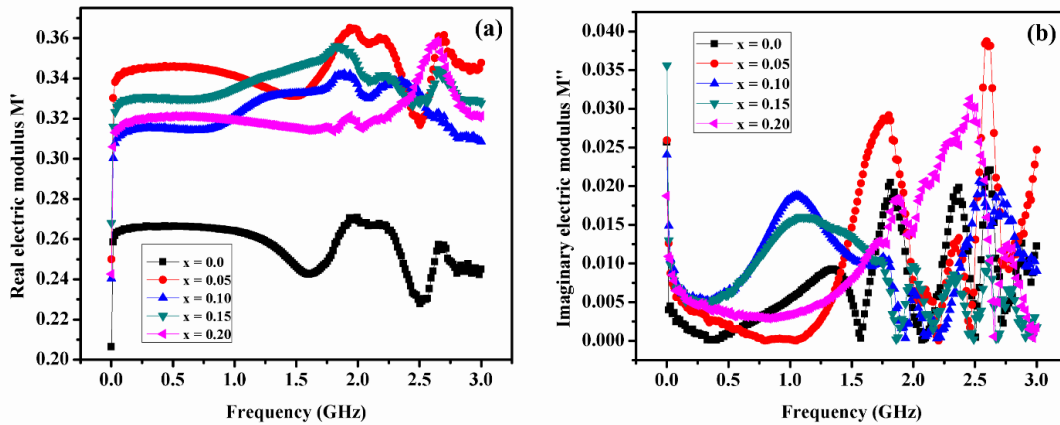


**Fig. 14.** Variations of (a) Real and (b) Imaginary electric modulus *versus* frequency

The Cole-Cole plot between  $M'$  and  $M''$  is illustrated in Fig. 15 (a)-(e), that delivers knowledge pertaining to grain and grain boundaries. It can be observed that all the plots showed single semicircle. The plot between  $M'$  and  $M''$  provides good information about semicircle. The semicircles at low frequency evident the resistance of grain and grain boundary, whereas the semicircles at high frequency are due to the resistance of grain only [62]. This is attributed to the

1  
2  
3  
4 presence of peaks in  $M''$  and the conduct of grain boundaries. It can be observed from  $M''$  versus  
5  
6  $M'$  plot that grain boundary density has a key role in conduction mechanism. The substitution of  
7  
8  $Ce^{3+}$  ions in Ni-Co ferrites enhanced the grain boundary resistance [40].  
9

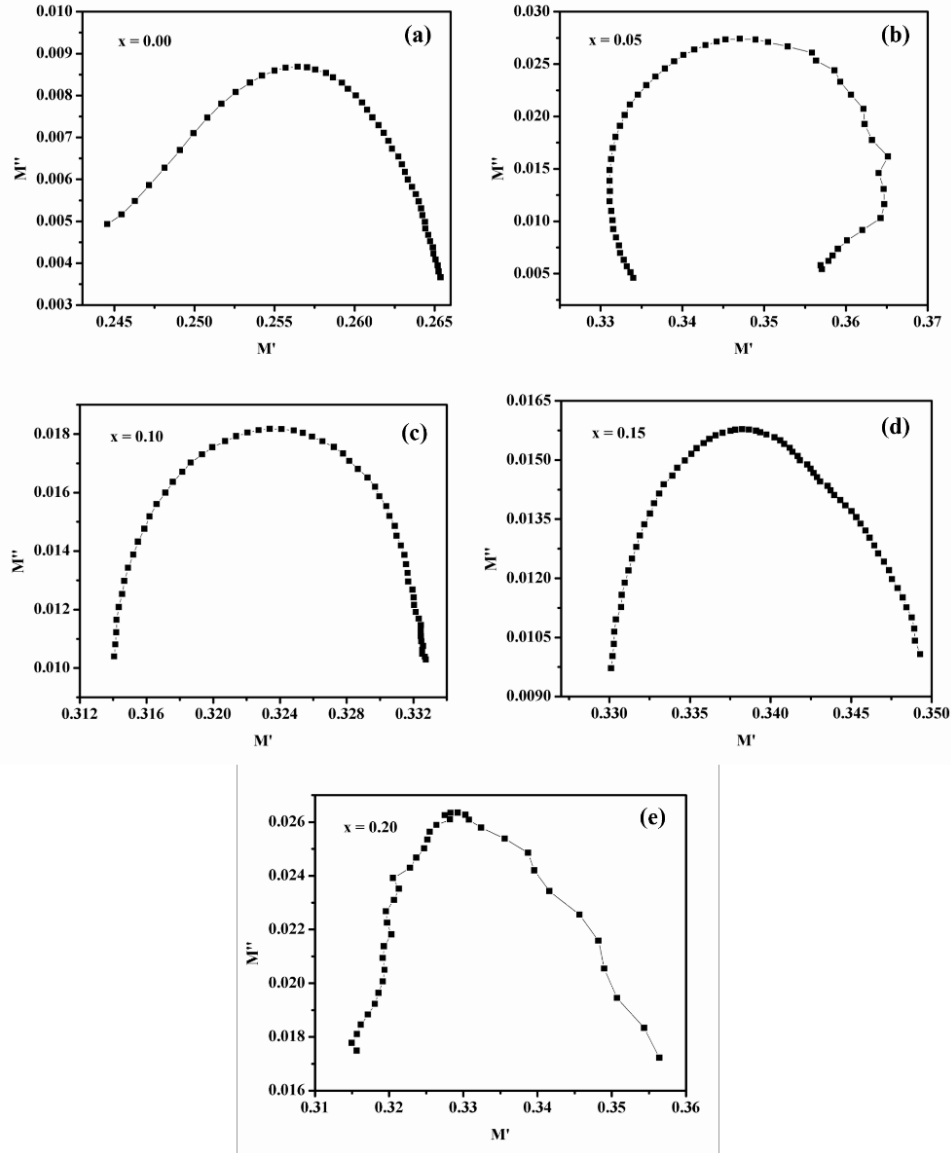


Fig. 15 (a)-(e). Cole-Cole plot of  $Ni_{0.3}Co_{0.7}Ce_xFe_{2-x}O_4$  ( $x = 0.0-0.20$ )

#### 4. Conclusions

54  
55 In this work  $Ce^{3+}$  substituted Ni-Co ferrites were prepared via sol-gel method. The FCC single  
56 phase spinel structure of ferrites was validated by XRD analysis. The crystalline size was  
57 calculated in 17.1-18.8 nm range. Hence these ferrites are synthesized in nano regime. Lattice  
58 parameter was observed to be significantly influenced by  $Ce^{3+}$  substitution and was lying between  
59  
60  
61  
62  
63  
64  
65

1  
2  
3  
4 8.363-8.374 Å in decreasing order. X-ray density was enhanced from 5.30-5.69 g/cm<sup>3</sup> with  
5  
6 increase in substitution. FTIR spectra revealed two prominent frequency bands and the force  
7  
8 constants showed increasing behavior with substitution. The microstructural studies revealed the  
9  
10 particle size on average was lying around 21.83 nm. The polycrystalline nature of ferrites was  
11  
12 validated by SAED distinctive rings pattern. EDX spectra confirmed the substitution of Ce<sup>3+</sup> ions.  
13  
14 The saturation magnetization and remanence reduced up to x = 0.10, then they increased for further  
15  
16 increase in substitution. The coercivity attained a maximum value of 908.93 Oe at x = 0.05.  
17  
18 Dielectric behavior of prepared ferrites showed decrease of dielectric parameters at low frequency.  
19  
20 Dielectric dispersion in ferrites is explained based on Maxwell Wagner interfacial polarization and  
21  
22 Koop's theory. The dielectric constant was reduced with increasing Ce<sup>3+</sup> substitution, for x = 0.20  
23  
24 its value was 3.02 at 1 GHz. At high frequency the dielectric loss in material was decreased  
25  
26 significantly. AC conductivity revealed an increasing behavior with applied frequency. The  
27  
28 imaginary electric modulus showed appearance of peak. The Cole-Cole graph expressed single  
29  
30 semicircle, which shows the conduction mechanism due to grain boundary density. All these  
31  
32 magnetic and dielectric traits of synthesized ferrites lead towards utilization in high frequency  
33  
34 devices, switching and memory storage devices fabrication.

### 34 **Acknowledgement**

35 The authors would like to acknowledge the Researcher's Supporting Project Number (RSP-  
36  
37 2021/269) King Saud University, Riyadh, Saudi Arabia, for their support in this work.  
38

### 39 **References**

- 40  
41 [1] M. Almessiere, B. Unal, Y. Slimani, H. Gungunes, M. Toprak, N. Tashkandi, *et al.*, "Effects of  
42  
43 Ce–Dy rare earths co-doping on various features of Ni–Co spinel ferrite microspheres prepared via  
44  
45 hydrothermal approach," *Journal of Materials Research and Technology*, vol. 14, pp. 2534-2553,  
46  
47 2021. <https://doi.org/10.1016/j.jmrt.2021.07.142>.  
48  
49 [2] M. Sarac, "Magnetic, structural, and optical properties of gadolinium-substituted Co<sub>0.5</sub>Ni<sub>0.5</sub>  
50  
51 Fe<sub>2</sub>O<sub>4</sub> spinel ferrite nanostructures," *Journal of Superconductivity and Novel Magnetism*, vol. 33,  
52  
53 pp. 397-406, 2020. <https://doi.org/10.1007/s10948-019-05359-3>.  
54  
55 [3] A. Baykal, N. Kasapoğlu, Y. Köseoğlu, A. C. Başaran, H. Kavas, and M. S. Toprak, "Microwave-  
56  
57 induced combustion synthesis and characterization of Ni<sub>x</sub>Co<sub>1-x</sub>Fe<sub>2</sub>O<sub>4</sub> nanocrystals (x= 0.0, 0.4,  
58  
59 0.6, 0.8, 1.0)," *Central European Journal of Chemistry*, vol. 6, pp. 125-130, 2008. DOI:  
60  
61 [10.2478/s11532-007-0070-4](https://doi.org/10.2478/s11532-007-0070-4).  
62  
63 [4] Y. Abbas, S. Mansour, M. Ibrahim, and S. E. Ali, "Microstructure characterization and cation  
64  
65 distribution of nanocrystalline cobalt ferrite," *Journal of magnetism and magnetic materials*, vol.  
66  
67 323, pp. 2748-2756, 2011. <https://doi.org/10.1016/j.jmmm.2011.05.038>.  
68  
69 [5] D. Pawar, P. P. Khirade, V. Vinayak, L. Ravangave, and S. Rathod, "Sol–gel auto-ignition  
70  
71 fabrication of Gd<sup>3+</sup> incorporated Ni<sub>0.5</sub>Co<sub>0.5</sub>Fe<sub>2</sub>O<sub>4</sub> multifunctional spinel ferrite nanocrystals  
72  
73 and its impact on structural, optical and magnetic properties," *SN Applied Sciences*, vol. 2, pp. 1-  
74  
75 12, 2020. <https://doi.org/10.1007/s42452-020-03505-4>.

- 1  
2  
3  
4 [6] V. Vinayak, P. P. Khirade, S. D. Birajdar, D. Sable, and K. Jadhav, "Structural, microstructural,  
5 and magnetic studies on magnesium (Mg<sup>2+</sup>)-substituted CoFe<sub>2</sub>O<sub>4</sub> nanoparticles," *Journal of*  
6 *Superconductivity and Novel Magnetism*, vol. 29, pp. 1025-1032, 2016. DOI [10.1007/s10948-015-](https://doi.org/10.1007/s10948-015-3348-3)  
7 [3348-3](https://doi.org/10.1007/s10948-015-3348-3).
- 8 [7] Raghvendra S. Yadav, J. Havlica, J. Masilko, L. Kalina, J. Wasserbauer, M. Hajdúchová, *et al.*,  
9 "Impact of Nd<sup>3+</sup> in CoFe<sub>2</sub>O<sub>4</sub> spinel ferrite nanoparticles on cation distribution, structural and  
10 magnetic properties," *Journal of Magnetism and Magnetic Materials*, vol. 399, pp. 109-117,  
11 2016/02/01/ 2016. <https://doi.org/10.1016/j.jmmm.2015.09.055>.
- 12 [8] O. Karaagac, B. Bilir, and H. Kockar, "Superparamagnetic cobalt ferrite nanoparticles: effect of  
13 temperature and base concentration," *Journal of Superconductivity and Novel Magnetism*, vol. 28,  
14 pp. 1021-1027, 2015. <http://dx.doi.org/10.1007/s10948-014-2798-3>.
- 15 [9] O. Karaagac, B. B. Yildiz, and H. Köçkar, "The influence of synthesis parameters on one-step  
16 synthesized superparamagnetic cobalt ferrite nanoparticles with high saturation magnetization,"  
17 *Journal of Magnetism and Magnetic Materials*, vol. 473, pp. 262-267, 2019/03/01/ 2019.  
18 <https://doi.org/10.1016/j.jmmm.2018.10.063>.
- 19 [10] N. M. Deraz and O. H. Abd-Elkader, "Processing and characterization of nano-magnetic  
20 Co<sub>0.5</sub>Ni<sub>0.5</sub>Fe<sub>2</sub>O<sub>4</sub> system," *Journal of Industrial and Engineering Chemistry*, vol. 20, pp. 3251-  
21 3255, 2014/09/25/ 2014. <https://doi.org/10.1016/j.jiec.2013.12.006>.
- 22 [11] S. Joshi, M. Kumar, S. Chhoker, G. Srivastava, M. Jewariya, and V. N. Singh, "Structural,  
23 magnetic, dielectric and optical properties of nickel ferrite nanoparticles synthesized by co-  
24 precipitation method," *Journal of Molecular Structure*, vol. 1076, pp. 55-62, 2014/11/05/ 2014.  
25 <https://doi.org/10.1016/j.molstruc.2014.07.048>.
- 26 [12] R. Nongjai, S. Khan, K. Asokan, H. Ahmed, and I. Khan, "Magnetic and electrical properties of In  
27 doped cobalt ferrite nanoparticles," *Journal of applied physics*, vol. 112, p. 084321, 2012.  
28 <https://doi.org/10.1063/1.4759436>.
- 29 [13] W. Zhu, L. Wang, R. Zhao, J. Ren, G. Lu, and Y. Wang, "Electromagnetic and microwave-  
30 absorbing properties of magnetic nickel ferrite nanocrystals," *Nanoscale*, vol. 3, pp. 2862-2864,  
31 2011. <https://doi.org/10.1039/C1NR10274E>.
- 32 [14] K. Mohit, V. R. Gupta, N. Gupta, and S. K. Rout, "Structural and microwave characterization of  
33 Ni<sub>0.2</sub>CoxZn<sub>0.8-x</sub>Fe<sub>2</sub>O<sub>4</sub> for antenna applications," *Ceramics International*, vol. 40, pp. 1575-  
34 1586, 2014/01/01/ 2014. <https://doi.org/10.1016/j.ceramint.2013.07.045>.
- 35 [15] A. Znidarsic, M. Limpel, and M. Drogenik, "Effect of dopants on the magnetic properties of MnZn  
36 ferrites for high frequency power supplies," *IEEE transactions on magnetics*, vol. 31, pp. 950-953,  
37 1995. DOI: [10.1109/20.364767](https://doi.org/10.1109/20.364767).
- 38 [16] L. Avazpour, H. Shokrollahi, M. R. Toroghinejad, and M. A. Zandi Khajeh, "Effect of rare earth  
39 substitution on magnetic and structural properties of Co<sub>1-x</sub>RE<sub>x</sub>Fe<sub>2</sub>O<sub>4</sub> (RE: Nd, Eu) nanoparticles  
40 prepared via EDTA/EG assisted sol-gel synthesis," *Journal of Alloys and Compounds*, vol. 662,  
41 pp. 441-447, 2016/03/25/ 2016. <https://doi.org/10.1016/j.jallcom.2015.11.188>.
- 42 [17] R. H. Kadam, K. Desai, V. S. Shinde, M. Hashim, and S. E. Shirsath, "Influence of Gd<sup>3+</sup> ion  
43 substitution on the MnCrFeO<sub>4</sub> for their nanoparticle shape formation and magnetic properties,"  
44 *Journal of Alloys and Compounds*, vol. 657, pp. 487-494, 2016/02/05/ 2016.  
45 <https://doi.org/10.1016/j.jallcom.2015.10.164>.
- 46 [18] D. Phugate, R. B. Borade, S. Kadam, L. Dhale, R. Kadam, S. E. Shirsath, *et al.*, "Effect of Ho<sup>3+</sup>  
47 Ion Doping on Thermal, Structural, and Morphological Properties of Co-Ni Ferrite Synthesized by  
48 Sol-Gel Method," *Journal of Superconductivity and Novel Magnetism*, vol. 33, pp. 3545-3554,  
49 2020. <https://doi.org/10.1007/s10948-020-05616-w>.
- 50 [19] M. F. Warsi, A. Iftikhar, M. A. Yousuf, M. I. Sarwar, S. Yousaf, S. Haider, *et al.*, "Erbium  
51 substituted nickel-cobalt spinel ferrite nanoparticles: Tailoring the structural, magnetic and  
52 electrical parameters," *Ceramics International*, vol. 46, pp. 24194-24203, 2020.  
53 <https://doi.org/10.1016/j.ceramint.2020.06.199>.
- 54  
55  
56  
57  
58  
59  
60  
61  
62  
63  
64  
65

- 1  
2  
3  
4 [20] V. G. Deonikar, V. D. Kulkarni, S. M. Rathod, and H. Kim, "Fabrication and characterizations of  
5 structurally engineered lanthanum substituted nickel-cobalt ferrites for the analysis of electric and  
6 dielectric properties," *Inorganic Chemistry Communications*, vol. 119, p. 108074, 2020.  
7 <https://doi.org/10.1016/j.inoche.2020.108074>.
- 8  
9 [21] M. Kokare, N. A. Jadhav, Y. Kumar, K. Jadhav, and S. Rathod, "Effect of Nd<sup>3+</sup> doping on  
10 structural and magnetic properties of Ni<sub>0.5</sub>Co<sub>0.5</sub>Fe<sub>2</sub>O<sub>4</sub> nanocrystalline ferrites synthesized by  
11 sol-gel auto combustion method," *Journal of Alloys and Compounds*, vol. 748, pp. 1053-1061,  
12 2018. <https://doi.org/10.1016/j.jallcom.2018.03.168>.
- 13 [22] M. A. Almessiere, Y. Slimani, I. A. Auwal, S. E. Shirsath, A. Manikandan, A. Baykal, *et al.*,  
14 "Impact of Tm<sup>3+</sup> and Tb<sup>3+</sup> Rare Earth Cations Substitution on the Structure and Magnetic  
15 Parameters of Co-Ni Nanospinel Ferrite," *Nanomaterials*, vol. 10, p. 2384, 2020.  
16 <https://doi.org/10.3390/nano10122384>.
- 17 [23] S. S. e. a. Satpute, "Substitution effect of Y<sup>3+</sup> ions on the structural, magnetic and electrical  
18 properties of cobalt ferrite nanoparticles.," *Cerâmica*, vol. v. 66, pp. pp. 43-49, 2020.  
19 <https://doi.org/10.1590/0366-69132020663772734>.
- 20 [24] V. More, R. B. Borade, K. Desai, V. K. Barote, S. Kadam, V. S. Shinde, *et al.*, "Site Occupancy,  
21 Surface Morphology and Mechanical Properties of Ce<sup>3+</sup> Added Ni-Mn-Zn Ferrite Nanocrystals  
22 Synthesized Via Sol-Gel Route," *NANO*, 2021. <https://doi.org/10.1142/S1793292021500594>.
- 23 [25] R. Arulmurugan, B. Jeyadevan, G. Vaidyanathan, and S. Sendhilnathan, "Effect of zinc substitution  
24 on Co-Zn and Mn-Zn ferrite nanoparticles prepared by co-precipitation," *Journal of Magnetism  
25 and Magnetic Materials*, vol. 288, pp. 470-477, 2005. <https://doi.org/10.1016/j.jmmm.2004.09.138>.
- 26 [26] N. Das, R. Majumdar, A. Sen, and H. S. Maiti, "Nanosized bismuth ferrite powder prepared through  
27 sonochemical and microemulsion techniques," *Materials Letters*, vol. 61, pp. 2100-2104, 2007.  
28 <https://doi.org/10.1016/j.matlet.2006.08.026>.
- 29 [27] S. Komarneni, E. Fregeau, E. Breval, and R. Roy, "Hydrothermal preparation of ultrafine ferrites  
30 and their sintering," *Journal of the American Ceramic Society*, vol. 71, pp. C- 26-C- 28, 1988.  
31 <https://doi.org/10.1111/j.1151-2916.1988.tb05773.x>.
- 32 [28] V. K. Mande, J. S. Kounsalye, S. Vyawahare, and K. Jadhav, "Effect of  $\gamma$ -radiation on structural,  
33 morphological, magnetic and dielectric properties of Zn-Cr substituted nickel ferrite  
34 nanoparticles," *Journal of Materials Science: Materials in Electronics*, vol. 30, pp. 56-68, 2019.  
35 <https://doi.org/10.1007/s10854-018-0252-1>.
- 36 [29] Z. Yue, J. Zhou, L. Li, H. Zhang, and Z. Gui, "Synthesis of nanocrystalline NiCuZn ferrite powders  
37 by sol-gel auto-combustion method," *Journal of Magnetism and magnetic materials*, vol. 208, pp.  
38 55-60, 2000. [https://doi.org/10.1016/S0304-8853\(99\)00566-1](https://doi.org/10.1016/S0304-8853(99)00566-1).
- 39 [30] K. Lohar, A. Pachpinde, M. Langade, R. Kadam, and S. E. Shirsath, "Self-propagating high  
40 temperature synthesis, structural morphology and magnetic interactions in rare earth Ho<sup>3+</sup> doped  
41 CoFe<sub>2</sub>O<sub>4</sub> nanoparticles," *Journal of alloys and compounds*, vol. 604, pp. 204-210, 2014.  
42 <https://doi.org/10.1016/j.jallcom.2014.03.141>.
- 43 [31] A. K. Nikumbh, R. A. Pawar, D. V. Nighot, G. S. Gugale, M. D. Sangale, M. B. Khanvilkar, *et al.*,  
44 "Structural, electrical, magnetic and dielectric properties of rare-earth substituted cobalt ferrites  
45 nanoparticles synthesized by the co-precipitation method," *Journal of Magnetism and Magnetic  
46 Materials*, vol. 355, pp. 201-209, 2014/04/01/ 2014. <https://doi.org/10.1016/j.jmmm.2013.11.052>.
- 47 [32] K. Tanbir, M. P. Ghosh, R. K. Singh, M. Kar, and S. Mukherjee, "Effect of doping different rare  
48 earth ions on microstructural, optical, and magnetic properties of nickel-cobalt ferrite  
49 nanoparticles," *Journal of Materials Science: Materials in Electronics*, vol. 31, pp. 435-443,  
50 2020/01/01 2020. <https://doi.org/10.1007/s10854-019-02546-9>.
- 51 [33] L. Shao, A. Sun, Y. Zhang, L. Yu, N. Suo, and Z. Zuo, "Comparative study on the structure and  
52 magnetic properties of Ni-Mg-Co ferrite doped with Al and rare earth elements," *Journal of  
53 Materials Science: Materials in Electronics*, vol. 32, pp. 5339-5352, 2021.  
54 <https://doi.org/10.1007/s10854-020-05161-1>.
- 55  
56  
57  
58  
59  
60  
61  
62  
63  
64  
65

- 1  
2  
3  
4 [34] A. B. Kadam, V. K. Mande, S. B. Kadam, R. H. Kadam, S. E. Shirsath, and R. B. Borade, "Influence  
5 of gadolinium (Gd<sup>3+</sup>) ion substitution on structural, magnetic and electrical properties of cobalt  
6 ferrites," *Journal of Alloys and Compounds*, vol. 840, p. 155669, 2020/11/05/ 2020.  
7 <https://doi.org/10.1016/j.jallcom.2020.155669>.
- 8 [35] M. Kokare, N. A. Jadhav, V. Singh, and S. Rathod, "Effect of Sm<sup>3+</sup> substitution on the structural  
9 and magnetic properties of Ni-Co nanoferrites," *Optics & Laser Technology*, vol. 112, pp. 107-116,  
10 2019. <https://doi.org/10.1016/j.optlastec.2018.10.045>.
- 11 [36] M. Arana, V. Galván, S. E. Jacobo, and P. G. Bercoff, "Cation distribution and magnetic properties  
12 of LiMnZn ferrites," *Journal of Alloys and Compounds*, vol. 568, pp. 5-10, 2013/08/15/ 2013.  
13 <https://doi.org/10.1016/j.jallcom.2013.03.068>.
- 14 [37] A. Aslam, N. Morley, N. Amin, M. I. Arshad, M. A. un Nabi, A. Ali, *et al.*, "Study of structural,  
15 optical and electrical properties of La<sup>3+</sup> doped Mg<sub>0.25</sub>Ni<sub>0.15</sub>Cu<sub>0.25</sub>Co<sub>0.35</sub>Fe<sub>2-x</sub>LaxO<sub>4</sub>  
16 spinel ferrites," *Physica B: Condensed Matter*, vol. 602, p. 412565, 2021.  
17 <https://doi.org/10.1016/j.physb.2020.412565>.
- 18 [38] M. Rahman, N. Hasan, M. Hoque, M. Hossen, and M. Arifuzzaman, "Structural, dielectric, and  
19 electrical transport properties of Al<sup>3+</sup> substituted nanocrystalline Ni-Cu spinel ferrites prepared  
20 through the sol-gel route," *Results in Physics*, p. 105610, 2022.  
21 <https://doi.org/10.1016/j.rinp.2022.105610>.
- 22 [39] B. P. Jacob, S. Thankachan, S. Xavier, and E. Mohammed, "Effect of Tb<sup>3+</sup> substitution on  
23 structural, electrical and magnetic properties of sol-gel synthesized nanocrystalline nickel ferrite,"  
24 *Journal of Alloys and Compounds*, vol. 578, pp. 314-319, 2013.  
25 <https://doi.org/10.1016/j.jallcom.2013.04.147>.
- 26 [40] A. Ditta, M. A. Khan, M. Junaid, R. A. Khalil, and M. F. Warsi, "Structural, magnetic and spectral  
27 properties of Gd and Dy co-doped dielectrically modified Co-Ni (Ni<sub>0.4</sub>Co<sub>0.6</sub>Fe<sub>2</sub>O<sub>4</sub>) ferrites,"  
28 *Physica B: Condensed Matter*, vol. 507, pp. 27-34, 2017.  
29 <https://doi.org/10.1016/j.physb.2016.11.030>.
- 30 [41] M. Y. Lodhi, K. Mahmood, A. Mahmood, H. Malik, M. F. Warsi, I. Shakir, *et al.*, "New Mg<sub>0.5</sub>  
31 CoxZn<sub>0.5-x</sub>Fe<sub>2</sub>O<sub>4</sub> nano-ferrites: structural elucidation and electromagnetic behavior  
32 evaluation," *Current Applied Physics*, vol. 14, pp. 716-720, 2014.  
33 <https://doi.org/10.1016/j.cap.2014.02.021>.
- 34 [42] M. Hashim, S. Kumar, S. E. Shirsath, R. Kotnala, J. Shah, and R. Kumar, "Synthesis and  
35 characterizations of Ni<sup>2+</sup> substituted cobalt ferrite nanoparticles," *Materials Chemistry and*  
36 *Physics*, vol. 139, pp. 364-374, 2013. <https://doi.org/10.1016/j.matchemphys.2012.09.019>.
- 37 [43] M. M. L. Sonia, S. Anand, V. M. Vinoseel, M. A. Janifer, S. Pauline, and A. Manikandan, "Effect  
38 of lattice strain on structure, morphology and magneto-dielectric properties of spinel NiGdxFe<sub>2-x</sub>  
39 O<sub>4</sub> ferrite nano-crystallites synthesized by sol-gel route," *Journal of Magnetism and Magnetic*  
40 *Materials*, vol. 466, pp. 238-251, 2018. <https://doi.org/10.1016/j.jmmm.2018.07.017>.
- 41 [44] M. Almessiere, Y. Slimani, A. D. Korkmaz, M. Sertkol, A. Baykal, I. Ercan, *et al.*, "Sonochemical  
42 synthesis of CoFe<sub>2-x</sub>NdxO<sub>4</sub> nanoparticles: structural, optical, and magnetic investigation,"  
43 *Journal of Superconductivity and Novel Magnetism*, vol. 32, pp. 3837-3844, 2019.  
44 <https://doi.org/10.1007/s10948-019-05147-z>.
- 45 [45] A. Maqsood, K. Khan, M. Anis-ur-Rehman, and M. Malik, "Spectroscopic and magnetic  
46 investigation of NiCo nanoferrites," *Journal of alloys and compounds*, vol. 509, pp. 7493-7497,  
47 2011. <https://doi.org/10.1016/j.jallcom.2011.04.092>.
- 48 [46] Z. Karimi, Y. Mohammadifar, H. Shokrollahi, S. K. Asl, G. Yousefi, and L. Karimi, "Magnetic and  
49 structural properties of nano sized Dy-doped cobalt ferrite synthesized by co-precipitation,"  
50 *Journal of Magnetism and Magnetic Materials*, vol. 361, pp. 150-156, 2014.  
51 <https://doi.org/10.1016/j.jmmm.2014.01.016>.
- 52 [47] L. Kumar and M. Kar, "Effect of La<sup>3+</sup> substitution on the structural and magnetocrystalline  
53 anisotropy of nanocrystalline cobalt ferrite (CoFe<sub>2-x</sub>LaxO<sub>4</sub>)," *Ceramics International*, vol. 38, pp.  
54 4771-4782, 2012/08/01/ 2012. <https://doi.org/10.1016/j.ceramint.2012.02.065>.
- 55  
56  
57  
58  
59  
60  
61  
62  
63  
64  
65

- 1  
2  
3  
4 [48] L. B. Tahar, M. Artus, S. Ammar, L. S. Smiri, F. Herbst, M. J. Vaulay, *et al.*, "Magnetic properties  
5 of CoFe<sub>1.9</sub>RE<sub>0.1</sub>O<sub>4</sub> nanoparticles (RE=La, Ce, Nd, Sm, Eu, Gd, Tb, Ho) prepared in polyol,"  
6 *Journal of Magnetism and Magnetic Materials*, vol. 320, pp. 3242-3250, 2008/12/01/ 2008.  
7 <https://doi.org/10.1016/j.jmmm.2008.06.031>.
- 8 [49] İ. Şabikoğlu, L. Paralı, O. Malina, P. Novak, J. Kaslik, J. Tucek, *et al.*, "The effect of neodymium  
9 substitution on the structural and magnetic properties of nickel ferrite," *Progress in Natural  
10 Science: Materials International*, vol. 25, pp. 215-221, 2015.  
11 <https://doi.org/10.1016/j.pnsc.2015.06.002>.
- 12 [50] M. Hashim, M. Raghasudha, S. S. Meena, J. Shah, S. E. Shirsath, S. Kumar, *et al.*, "Influence of  
13 rare earth ion doping (Ce and Dy) on electrical and magnetic properties of cobalt ferrites," *Journal  
14 of Magnetism and Magnetic Materials*, vol. 449, pp. 319-327, 2018.  
15 <https://doi.org/10.1016/j.jmmm.2017.10.023>.
- 16 [51] S. Hassanzadeh-Tabrizi, S. Behbahanian, and J. Amighian, "Synthesis and magnetic properties of  
17 NiFe<sub>2</sub>-xSmxO<sub>4</sub> nanopowder," *Journal of Magnetism and Magnetic Materials*, vol. 410, pp. 242-  
18 247, 2016. <https://doi.org/10.1016/j.jmmm.2016.03.015>.
- 19 [52] M. A. Almessiere, Y. Slimani, and A. Baykal, "Synthesis and characterization of Co<sub>1</sub>-  
20 2xNi<sub>x</sub>MnxCeyFe<sub>2</sub>-yO<sub>4</sub> nanoparticles," *Journal of Rare Earths*, vol. 38, pp. 188-194, 2020.  
21 <https://doi.org/10.1016/j.jre.2019.07.005>.
- 22 [53] G. Xi, T. Zhao, L. Wang, C. Dun, and Y. Zhang, "Effect of doping rare earths on magnetostriction  
23 characteristics of CoFe<sub>2</sub>O<sub>4</sub> prepared from spent Li-ion batteries," *Physica B: Condensed Matter*,  
24 vol. 534, pp. 76-82, 2018. <https://doi.org/10.1016/j.physb.2018.01.036>.
- 25 [54] A. Pachpinde, M. Langade, K. Lohar, S. Patange, and S. E. Shirsath, "Impact of larger rare earth  
26 Pr<sup>3+</sup> ions on the physical properties of chemically derived Pr<sub>x</sub>CoFe<sub>2</sub>-xO<sub>4</sub> nanoparticles,"  
27 *Chemical physics*, vol. 429, pp. 20-26, 2014. <https://doi.org/10.1016/j.chemphys.2013.11.018>.
- 28 [55] A. Kadam, S. Shinde, S. Yadav, P. Patil, and K. Rajpure, "Structural, morphological, electrical and  
29 magnetic properties of Dy doped Ni-Co substitutional spinel ferrite," *Journal of Magnetism and  
30 Magnetic materials*, vol. 329, pp. 59-64, 2013. <https://doi.org/10.1016/j.jmmm.2012.10.008>.
- 31 [56] R. Kambale, "NR Adhate, BK Chougule, Yd Kolekar, "Magnetic and dielectric properties of mixed  
32 spinel Ni-Zn ferrites synthesized by citrate nitrate combustion method", "*J. Alloys Compd*, vol.  
33 507, pp. 372-377, 2010. <https://doi.org/10.1016/j.jallcom.2009.10.187>.
- 34 [57] R. S. Devan, Y. D. Kolekar, and B. K. Chougule, "Effect of cobalt substitution on the properties of  
35 nickel-copper ferrite," *Journal of Physics: Condensed Matter*, vol. 18, pp. 9809-9821, 2006/10/13  
36 2006. <https://doi.org/10.1088/0953-8984/18/43/004>.
- 37 [58] M. Ishaque, M. U. Islam, M. Azhar Khan, I. Z. Rahman, A. Genson, and S. Hampshire, "Structural,  
38 electrical and dielectric properties of yttrium substituted nickel ferrites," *Physica B: Condensed  
39 Matter*, vol. 405, pp. 1532-1540, 2010/03/15/ 2010. <https://doi.org/10.1016/j.physb.2009.12.035>.
- 40 [59] H. S. Aziz, S. Rasheed, R. A. Khan, A. Rahim, J. Nisar, S. M. Shah, *et al.*, "Evaluation of electrical,  
41 dielectric and magnetic characteristics of Al-La doped nickel spinel ferrites," *RSC advances*, vol.  
42 6, pp. 6589-6597, 2016. <https://doi.org/10.1039/C5RA20981A>.
- 43 [60] J. H. Joshi, D. K. Kanchan, M. J. Joshi, H. O. Jethva, and K. D. Parikh, "Dielectric relaxation,  
44 complex impedance and modulus spectroscopic studies of mix phase rod like cobalt sulfide  
45 nanoparticles," *Materials Research Bulletin*, vol. 93, pp. 63-73, 2017/09/01/ 2017.  
46 <https://doi.org/10.1016/j.materresbull.2017.04.013>.
- 47 [61] M. A. Iqbal, M. Islam, I. Ali, I. Sadiq, and I. Ali, "High frequency dielectric properties of Eu<sup>3+</sup>-  
48 substituted Li-Mg ferrites synthesized by sol-gel auto-combustion method," *Journal of Alloys and  
49 Compounds*, vol. 586, pp. 404-410, 2014. <https://doi.org/10.1016/j.jallcom.2013.10.066>.
- 50 [62] D. Varshney and K. Verma, "Substitutional effect on structural and dielectric properties of  
51 Ni<sub>1-x</sub>A<sub>x</sub>Fe<sub>2</sub>O<sub>4</sub> (A = Mg, Zn) mixed spinel ferrites," *Materials Chemistry and Physics*, vol. 140,  
52 pp. 412-418, 2013/06/15/ 2013. <https://doi.org/10.1016/j.matchemphys.2013.03.062>.
- 53  
54  
55  
56  
57  
58  
59  
60  
61  
62  
63  
64  
65

**Declaration of competing interest**

The authors declare that they have no known competing financial interests or personal relationships that could have appeared to influence the work reported in this paper.